AGU ADVANCING EARTH AND SPACE SCIENCE

Geophysical Research Letters

RESEARCH LETTER
10.1029/2022GL098779

Thunderstorm Activity Under Intermediate and Extreme Climate Change Scenarios

Alex M. Haberlie[1], Walker S. Ashley[1], Christopher M. Battisto[1], and Vittorio A. Gensini[1]

[1]Department of Earth, Atmosphere, and Environment, Northern Illinois University, DeKalb, IL, USA

Key Points:

- A regional climate model is used to simulate two climate change scenarios
- Fewer Southern Plains thunderstorm days, more in the Midwest and Southeast
- Some increases in conditional instability are offset by convective inhibition

Supporting Information:

Supporting Information may be found in the online version of this article.

Correspondence to:

A. M. Haberlie,
ahaberlie1@niu.edu

Citation:

Haberlie, A. M., Ashley, W. S., Battisto, C. M., & Gensini, V. A. (2022). Thunderstorm activity under intermediate and extreme climate change scenarios. *Geophysical Research Letters*, *49*, e2022GL098779. https://doi.org/10.1029/2022GL098779

Received 28 MAR 2022
Accepted 21 JUN 2022

Author Contributions:

Conceptualization: Alex M. Haberlie, Walker S. Ashley
Data curation: Alex M. Haberlie, Vittorio A. Gensini
Formal analysis: Alex M. Haberlie, Christopher M. Battisto
Funding acquisition: Alex M. Haberlie, Walker S. Ashley, Vittorio A. Gensini
Investigation: Alex M. Haberlie, Christopher M. Battisto
Methodology: Alex M. Haberlie, Christopher M. Battisto
Project Administration: Alex M. Haberlie, Walker S. Ashley, Vittorio A. Gensini
Resources: Alex M. Haberlie, Walker S. Ashley, Vittorio A. Gensini
Software: Alex M. Haberlie, Christopher M. Battisto, Vittorio A. Gensini
Supervision: Alex M. Haberlie
Validation: Alex M. Haberlie
Visualization: Alex M. Haberlie

Abstract Assessing how increasing greenhouse gas concentrations may modify regional climates is an ongoing challenge. Relatively little work has examined how climate change may influence processes related to regional thunderstorm activity. This is important to consider in areas where thunderstorms are important for maintaining regional hydroclimates. This study focuses on three convection-allowing climate simulations—namely, a retrospective simulation (1990–2005) and two possible climate change scenarios (2085–2100)—with domains encompassing the conterminous United States. Regional and seasonal variability is noted in the response of thunderstorm activity as measured by thresholds in simulated radar reflectivity factor in the two climate change scenarios. A decrease in thunderstorm activity is projected for the Southern Plains, whereas the Southeast and Midwest experience an increase in thunderstorm activity. An examination of environmental parameters related to thunderstorm activity reveals an overall increase in convective instability but spatially varying changes in convective inhibition.

Plain Language Summary More favorable conditions may exist for thunderstorm activity throughout the United States in the late 21st century. However, certain factors prevent thunderstorms from taking advantage of these conditions by suppressing their formation. This leads to a varying response to possible climate change scenarios, with less thunderstorm activity in the Great Plains, and more in the Midwest and Southeast.

1. Introduction

For decades, climate scientists have been aware of the relationship between temperature and greenhouse gases, and have attributed increasing concentrations of these gases (e.g., carbon dioxide, methane) to human activity (Callendar, 1938). Over that time, many studies have verified the positive relationship between GHGs and global mean temperature and precipitation (Hartmann, 2015). However, regional responses to climate change have been found to be more complex and variable (Pachauri et al., 2014). Compounding this issue, atmospheric processes pertinent to regional climate are not resolved by global climate models (GCMs) due to their relatively sparse computational grids (Prein et al., 2015). The initiation and maintenance of thunderstorms, for example, relies heavily on meso-γ ($\sim$10 km) scale processes—which is an order of magnitude smaller than typical GCM grids—related to land cover, terrain, moisture flux, and transient baroclinity (Trapp, 2013). Since thunderstorms are affiliated with numerous benefits and hazards, climate modeling that more accurately simulates thunderstorms and potential changes in their frequency is of interest to society. Thus, climate change research has incorporated an increasingly local perspective over the past decade by explicitly simulating mesoscale processes (Kendon et al., 2021; Prein et al., 2015; Takayabu et al., 2021).

Regional thunderstorm activity can be implicitly approximated in coarse resolution GCMs by examining variables like convective available potential energy (CAPE; J kg^{-1}) and convective inhibition (CIN; J kg^{-1}). Using an ingredients-based approach (Brooks et al., 2003; Doswell & Schultz, 2006; McNulty, 1995), these variables are used as proxies of atmospheric conditions that may be favorable for thunderstorm development (herein, thunderstorm environments). The body of literature on thunderstorm environments in reanalysis datasets is substantial (Allen, 2018; Brooks, 2013; Brooks et al., 2019; Gensini et al., 2014). Trends in thunderstorm environments have also been examined at length, both in reanalysis datasets (Gensini & Brooks, 2018; Riemann-Campe et al., 2009; Tang et al., 2019; Taszarek, Allen, Brooks, et al., 2021; Taszarek, Allen, Marchio, & Brooks, 2021) and GCM output (Diffenbaugh et al., 2013; Lepore et al., 2021; Trapp et al., 2009; Trapp, Diffenbaugh, et al., 2007). In general, these studies have reported either observed or projected increases in instability over time, which suggests an attendant increase in thunderstorm activity in the 21st century (Gensini, 2021). However, a crucial limitation

Writing – original draft: Alex M. Haberlie, Walker S. Ashley, Christopher M. Battisto
Writing – review & editing: Alex M. Haberlie, Walker S. Ashley, Christopher M. Battisto, Vittorio A. Gensini

of these works is that GCMs and other coarse resolution models cannot resolve individual thunderstorms and important mesoscale processes that lead to their development (Kendon et al., 2021).

Higher resolution climate simulations, conducted using a process called dynamical downscaling (Trapp, Halvorson, & Diffenbaugh, 2007), instead use GCM output as initial and boundary conditions to inform a regional climate model (RCM). RCMs with a grid spacing of ≤4 km permit explicit simulations of convective processes (Prein et al., 2015; Weisman et al., 1997), and individual thunderstorms can be identified in the resulting model output. While global domains at these resolutions are rapidly becoming more feasible (Gensini & Mote, 2014; Kendon et al., 2021; Trapp et al., 2011), high computational and storage demands have limited the temporal and spatial scope of these simulations. Existing experiments have study periods of 10–30 years, subcontinental domains, and use one GCM and/or climate change scenario. However, these studies have provided more details about potential changes in thunderstorm activity (Gensini & Mote, 2015; Hoogewind et al., 2017; Rasmussen et al., 2020; Trapp et al., 2019). For example, Rasmussen et al. (2020) illustrates potential limitations of thunderstorm environment studies—namely, despite the widespread increases in CAPE, there was a spatially varied response in thunderstorm activity. However, these disparities may be due to reported model biases (Liu et al., 2017).

2. Experiment Setup

Initial and boundary conditions for the RCM are informed by a bias-corrected (Bruyère et al., 2014) and regridded version of the Community Earth System Model (CESM; Hurrell et al. [2013]) output. Specifically, 6-hourly output from 1990 to 2005 and 2085 to 2100 are accessed for this work (Monaghan et al., 2014). For the end-of-21st-century period, we use bias-corrected CESM data for Representative Concentration Pathway (RCP; Moss et al., 2010) 4.5 and 8.5. The goal of using two RCPs is to examine and compare regional responses to an intermediate (RCP 4.5) and extreme (RCP 8.5) climate change scenario. These three periods are passed into WRF-ARW version 4.1.2 (Skamarock et al., 2019), and the corresponding 15-year simulations are run on a domain fully containing the conterminous United States (CONUS). The RCM uses a grid point spacing of 3.75 km, which permits the model to explicitly simulate deep, moist convective systems and other mesoscale processes important for thunderstorm development and sustenance (Kendon et al., 2021). 15 hydrologic years (1 Oct - 30 Sep) are simulated with continuous integration for each of the three periods—with spectral nudging (Miguez-Macho et al., 2004) of large (~2,000 km) features every 6 hr—resulting in hourly data output from 45 total simulations. Herein, the groups of simulations are referred to as **HIST** (1990–2005), **FUTR 4.5** (2085–2100, RCP 4.5), and **FUTR 8.5** (2085–2100, RCP 8.5). More information on this approach can be found in Gensini et al. (2022). This work will examine CAPE, CIN, and the spatiotemporal frequency of days with thunderstorms to reveal what, if any, differences exist between simulations representing a retrospective period and two possible future climate change scenarios.

3. Quantifying Thunderstorm Activity

Remote sensing platforms are commonly used to detect the occurrence of thunderstorms. These platforms include lightning locating systems (Cummins & Murphy, 2009), geostationary satellites (Menzel & Purdom, 1994), and radar (Serafin & Wilson, 2000). NEXRAD—the current weather radar platform in the United States—has been used for decades to detect thunderstorms for operational (Serafin & Wilson, 2000) and climatological (Fabry et al., 2017) applications. For the purposes of this study, model derived radar reflectivity factor (herein, simulated reflectivity) is used as a surrogate for the observed reflectivity data product provided by NEXRAD (Klazura & Imy, 1993). Simulated reflectivity produced by WRF is calculated using the simulated density of hydrometeors at a particular model level and time step (Creighton et al., 2014; Stoelinga, 2005), and this is analogous to the process used by NEXRAD. That said, disparities between simulated and observed reflectivity exist, and may be caused by different vertical and horizontal grid spacing, model assumptions about the shape and phase of hydrometeors (Stoelinga, 2005), and by noise and range-based issues experienced by NEXRAD (Smith et al., 1996). Despite these issues, previous work has used simulated reflectivity to examine changes in thunderstorm activity in a convection-allowing climate modeling context (e.g., Rasmussen et al., 2020; Trapp et al., 2019).

Three thresholds—40, 50, and 60 dBZ—are applied to the hourly simulation data to capture various intensities of simulated thunderstorm activity. The 40 dBZ threshold is commonly used for detecting thunderstorms in observed and simulated radar reflectivity (Fabry et al., 2017; Gensini & Mote, 2015; Parker & Knievel, 2005;

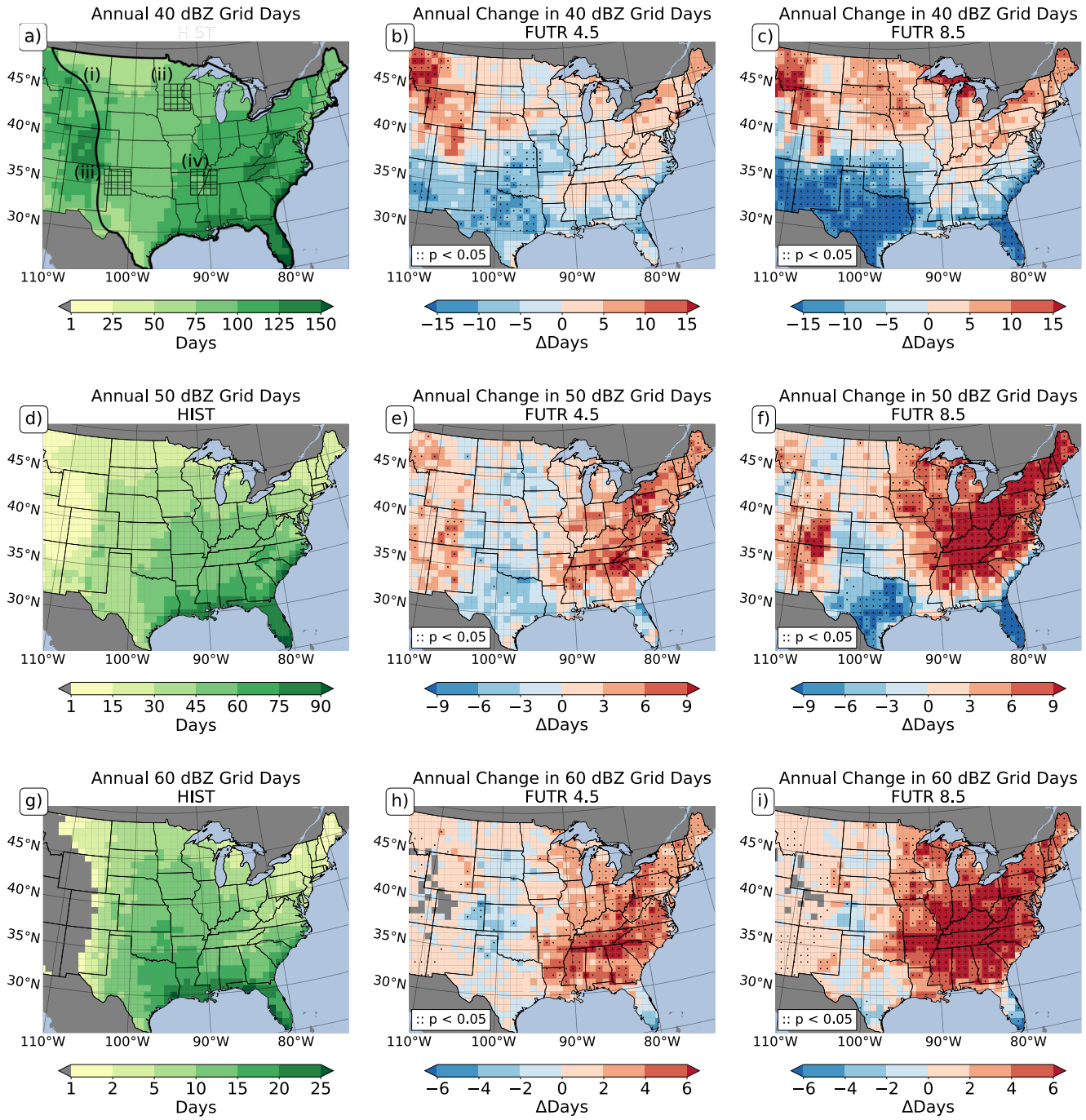

Figure 1. Mean annual grid days (starting at 12:00 UTC) for simulated reflectivity factor exceeding (a–c) 40 dBZ, (d–f) 50 dBZ, and (g–i) 60 dBZ. Absolute days are reported for HIST (a, d, and g) and differences relative to HIST are reported for (b, e, and h) FUTR 4.5, and (c, f, and i) FUTR 8.5. Significant differences between HIST and the respective FUTR period are denoted by stippling ($p < 0.05$; Mann-Whitney U test). Regions of interest are identified in (a), and include (i) the Contiguous United States east of the continental divide (ECONUS; black outline), and 16 grid cells near (ii) Minneapolis, MN, (iii) Amarillo, TX, and (iv) Memphis, TN.

Trapp et al., 2019), whereas 50 and 60 dBZ values are associated with stronger thunderstorms and the potential for hail (Ashley et al., 2012; Blair et al., 2011; Gensini & Mote, 2015; Ortega, 2018). The hourly data are then aggregated into days starting and ending at 12:00 UTC to calculate "thunderstorm day" (Changnon & Changnon, 2001; Trapp et al., 2019), herein "grid day," frequencies. Each analysis grid of 80 × 80 km (Figure 1; grid size used by NOAA for severe thunderstorm verification) is considered to have experienced a grid day if at least one 40 dBZ value occurred within its boundaries, and this process is repeated for the 50 and 60 dBZ thresholds. HIST, FUTR

4.5, and FUTR 8.5 mean annual and seasonal frequencies are then calculated by aggregating grid day results into their respective 15 year periods. To further examine annual cycles in grid day frequencies, grids are stratified into four regions identified in Figure 1a—namely, the eastern CONUS (961 grid cells), and 16-grid clusters centered on three cities (Minneapolis, MN; Amarillo, TX; and Memphis, TN). The study region is focused on areas of the CONUS east of the continental divide because this is where most U.S. thunderstorms (Changnon, 2001) and particularly intense/severe thunderstorms (Gensini & Ashley, 2011; Taszarek et al., 2020) occur. The results of the regional analyses are reported as regional means by dividing the sum of grid days within all regional grid cells by the count of grid cells within each region.

4. Changes in Thunderstorm Days

For all thresholds tested, mean annual grid days from HIST are generally highest in the southeast and decrease toward the north and west (Figure 1). For the eastern CONUS, HIST mean annual grid days range from 50 to 150 for 40 dBZ, whereas 60 dBZ grid days range from <1 to 25 per year. HIST 50 dBZ grid days range from 90 in Florida to 15 per year in the Northern Plains, and the spatial patterns and magnitudes are similar to observations of days with thunder (Changnon & Changnon, 2001) and lightning (Koehler, 2020). The correlation between higher grid day counts and distance to the Gulf is stronger for the 50 and 60 dBZ thresholds, whereas 40 dBZ grid days for the eastern Rocky Mountains occur just as often as parts of the Mississippi River Valley. The spatial pattern of 60 dBZ grid days matches those reported by studies that have examined extreme (i.e., return intervals ≥50 years) 1-hr rainfall totals (Stevenson & Schumacher, 2014).

For both FUTR 4.5 and FUTR 8.5, there is a significant decrease in 40 dBZ grid days in the Southern Plains. For both scenarios, broad areas of Texas, Oklahoma, and New Mexico experience at least five fewer 40 dBZ grid days per year in FUTR 4.5 and 10–15 fewer grid days per year in FUTR 8.5. In contrast, most changes are not significant over Florida and coastal regions of the Carolinas in FUTR 4.5, but they are in FUTR 8.5, with differences similar to those in Texas. In both scenarios, a marked north/south dichotomy exists across the eastern CONUS, with attendant increases of 40 dBZ grid days over the Northern Plains, Midwest, and Northeast. Interestingly, significant differences are limited to parts of the Northeast in RCP 4.5, whereas they are more widespread across the Northern Plains and northern Mississippi River Valley in FUTR 8.5. The largest changes are seen in FUTR 8.5, where five to 15 more 40 dBZ days are projected over parts of the Great Lakes, Northern Plains, and Northeast. For the higher thresholds, many areas east of the High Plains experience a significant increase in grid days, particularly in FUTR 8.5. In contrast, the High Plains generally see no significant changes, or significantly fewer days. Interestingly, parts of the southern and eastern Plains experience significant increases in 60 dBZ days, while experiencing significantly fewer 40 dBZ days. The Tennessee, Ohio, and Upper Mississippi River Valleys exhibit increases of three to over nine 50 dBZ grid days per year, whereas Texas and Florida may experience decreases in grid days of similar magnitudes. For 60 dBZ, the significant decreases in Texas and Florida largely disappear, whereas the areas of significant increases in 50 dBZ grid days are expanded southward and westward. Notably, portions of the Mid-South experience increases of up to six or more 60 dBZ grid days per year in both FUTR 4.5 and FUTR 8.5.

The cumulative annual sum of grid days within each region is calculated to compare year-to-year differences between regions and climate change scenarios relative to HIST. These values are reported as the mean cumulative annual grid days by dividing this sum by the count of grids within each region (Figure 2). For the eastern CONUS (Figures 2a–2c), the count of 40 dBZ grid days per year is similar for HIST, FUTR 4.5, and FUTR 8.5, with mean differences of less than one day per year. For the higher thresholds, mean yearly grid day counts for HIST are 43.9 days for 50 dBZ and 10.6 days for 60 dBZ. On the other hand, 50 (60) dBZ mean grid days are 45.3 (12.1) and 46.6 (13.7) per year for RCP 4.5 and RCP 8.5, respectively. This pattern was not consistent across the eastern CONUS. For example, Minneapolis (Figures 2d–2f), on average, experiences over six more 40 dBZ grid days per year in FUTR 8.5 compared to HIST, whereas Amarillo (Figures 2g–2i) experiences 12 fewer 40 dBZ grid days per year in FUTR 8.5. In contrast with Minneapolis, ECONUS, Amarillo, and Memphis all experience decreases in 40 dBZ days in both FUTR 4.5 and FUTR 8.5. For higher thresholds, the responses to the climate change scenarios are more complex. For Minneapolis, the mean annual 50 and 60 dBZ grid days are similar for HIST and FUTR 4.5, but higher for FUTR 8.5. On the other hand, mean annual 60 dBZ grid day counts for HIST and FUTR 8.5 are higher than FUTR 4.5 for the Amarillo region. The most dramatic differences between lower and

10.1029/2022GL098779

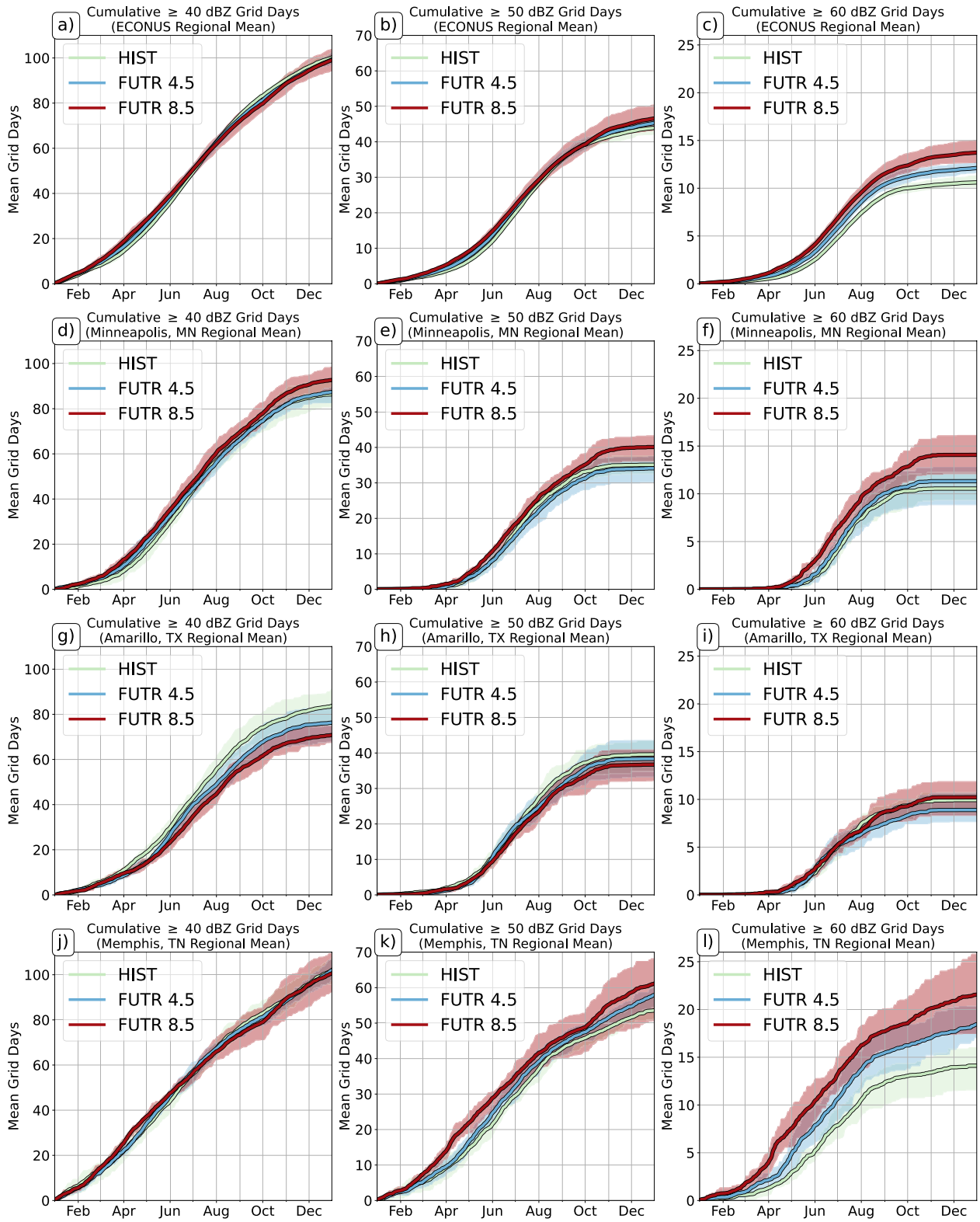

Figure 2. Cumulative annual sum of mean grid day (starting at 12:00 UTC) counts for grid cells in the regions identified in Figure 1—namely: (a–c) ECONUS, (d–f) Minneapolis, MN, (g–i) Amarillo, TX, and (j–l) Memphis, TN. Day counts are stratified into those with simulated reflectivity factor exceeding (first column) 40 dBZ, (second column) 50 dBZ, and (third column) 60 dBZ. Annual means (lines) and 25th to 75th percentile range (filled) are delineated for HIST (light green), FUTR 4.5 (blue), and FUTR 8.5 (dark red). Mean grid day counts are calculated by dividing the sum of grid days in a region by the regional grid cell count (i.e., 961 for ECONUS and 16 for Minneapolis, MN, Amarillo, TX, and Memphis, TN).

higher thresholds are illustrated in the Memphis region (Figures 2j–2l), where FUTR 4.5 (FUTR 8.5) produces 4.3 (7.4) more mean annual 60 dBZ grid days compared to HIST.

To examine sub-annual variability, regional mean grid day counts are stratified by season (Figure 3). For the eastern CONUS (Figures 3a–3c), there were increases (some significant) in grid days during the winter (DJF), spring (MAM), and fall (SON) for FUTR 4.5 and FUTR 8.5, whereas there were robust decreases during the summer (JJA). For DJF, significantly more 40 dBZ grid days are noted in both FUTR 4.5 (+1.7) and FUTR 8.5 (+2.7). There were significantly more MAM 50 dBZ grid days (+1.4 in FUTR 4.5 and +2.1 in FUTR 8.5) and 60 dBZ grid days (+0.7 in FUTR 4.5 and +1.4 in FUTR 8.5). Conversely, Significant decreases in JJA 40 dBZ grid days relative to HIST exist in both FUTR 4.5 (−3.5) and FUTR 8.5 (−5.8). This is also the case for JJA 50 dBZ grid days, of which there are 1.5 fewer days in FUTR 4.5 and 2.6 fewer days in FUTR 8.5, while there are only significantly more JJA 60 dBZ grid days for FUTR 8.5 (+0.7).

The largest and most robust changes across all regions and seasons occurred in the Memphis grid cluster (Figures 3j–3l) during MAM. Both FUTR 4.5 and FUTR 8.5 produced significantly more MAM 50 dBZ grid days (+3.2 and +5.3, respectively) and MAM 60 dBZ grid days (+2.4 and +4.2, respectively). In fact, for the Memphis cluster, there were almost twice as many MAM 60 dBZ grid days in FUTR 8.5 (8.7) compared to HIST (4.5). On an annual basis, MAM increases for the Memphis cluster are partially offset by decreases (none significant) in FUTR 4.5 and 8.5 during JJA for both 40 dBZ grid days (−3.3 and −6.8, respectively) and 50 dBZ grid days (−1.8 and −4.4, respectively), while JJA 60 dBZ grid day counts show small positive changes for FUTR 4.5 (+0.4) and FUTR 8.5 (+0.2). For the 16 grids centered on Minneapolis (Figures 3d–3f), there was little or no change under FUTR 4.5. However, under FUTR 8.5, MAM and SON counts of days with 50 dBZ occurrences (+2.3 and +3.1, respectively) and 60 dBZ occurrences (+1.5 and +1.3, respectively) increased significantly. The Amarillo grid cluster (Figures 3g–3i) experiences significant DJF decreases in 40 dBZ grid days (−2.4), 50 dBZ grid days (−0.6), and 60 dBZ grid days (−0.04) for FUTR 4.5, but no significant differences for FUTR 8.5.

5. Changes in CAPE and CIN

Since conditional instability is an ingredient necessary for thunderstorm formation (McNulty, 1995), mean seasonal MU (most unstable layer in the lowest 180 hPa) CAPE and MU CIN (herein, MU CAPE and MU CIN) are compared between HIST and the two climate change scenarios (Diffenbaugh et al., 2013). The "most unstable" versions of these measures of stability are used to account for both surface-based and elevated thunderstorm activity (Geerts et al., 2017). Study region MU CAPE values for HIST are lowest in DJF (0 to over 50 J kg^{-1}) and highest in JJA (50 to over 300 J kg^{-1}), and are comparable to results presented in previous works (Chen et al., 2020; Gensini & Ashley, 2011; Rasmussen et al., 2020; Taszarek, Allen, Brooks, et al., 2021; Trapp, Diffenbaugh, et al., 2007). Regionally, MU CAPE maximizes along the Gulf of Mexico and decreases toward the north and west. MU CIN, however, maximizes in the Great Plains, likely driven by the regular advection of an elevated mixed layer from the western United States (Trapp, 2013).

For all seasons in both climate change scenarios, the study region generally experiences increases in MU CAPE, and increases are larger in FUTR 8.5 compared to FUTR 4.5. The largest changes in MU CAPE occur in JJA (Figures 4g–4i), where areas of the Mid-South experience changes of ≥100 J kg^{-1} in FUTR 4.5, and ≥200 J kg^{-1} in FUTR 8.5 by the end of the century. This area is part of an axis of relatively large changes in MU CAPE from the Dakotas to the Carolina coast in both climate change scenarios. The June–August period is also when MU CIN exhibits the largest increases, with areas of the Northern Plains and Midwest experiencing changes of ≤−25 J kg^{-1} in FUTR 4.5. For FUTR 8.5, however, the vast majority of ECONUS experiences changes in MU CIN of ≤−25 J kg^{-1}, with some parts of the Great Plains experiencing changes in MU CIN of ≤−50 J kg^{-1}. The largest changes in MU CAPE during the MAM period (Figures 4d–4f) occur in southern Texas (≥150 J kg^{-1}) and the Mid-South (≥50 –≥ 100 J kg^{-1}). However, MU CIN changes of ≤−25 J kg^{-1} and ≤−50 J kg^{-1} are confined to the Southern Plains. DJF (Figures 4a–4c) and SON (Figures 4j–4l) exhibit more modest changes in MU CAPE, with fall increases in FUTR 4.5 (FUTR 8.5) ranging from 1 to 50 J kg^{-1} (1–150 J kg^{-1}), and winter increases in FUTR 4.5 (FUTR 8.5) up to 25 J kg^{-1} (50 J kg^{-1}). These results suggest that observed increases in both CAPE and CIN (Taszarek, Allen, Brooks, et al., 2021) may continue during the 21st century.

10.1029/2022GL098779

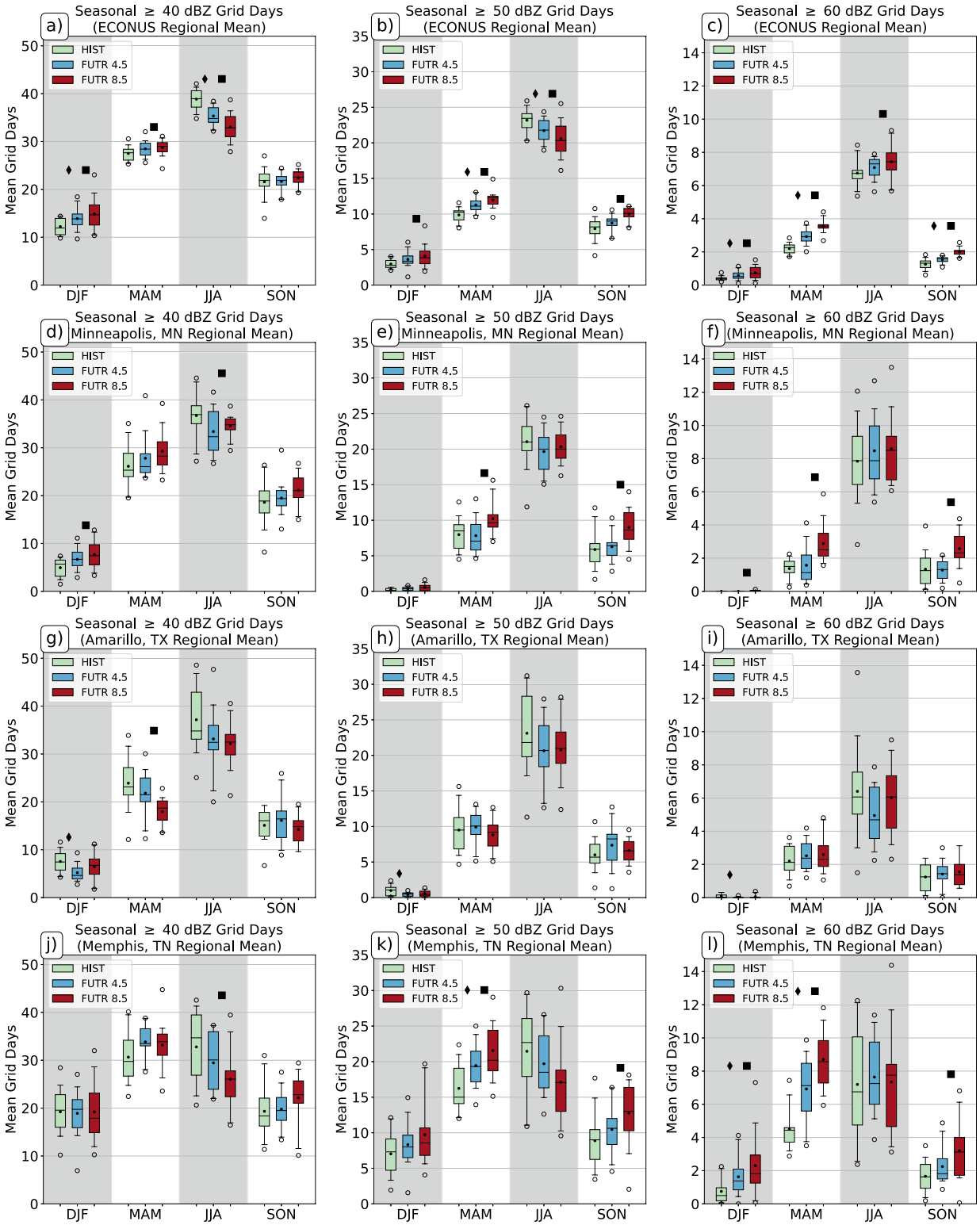

Figure 3. As in Figure 2, except regional distributions of seasonal grid days during 15 respective simulation years (HIST, FUTR 4.5, and FUTR 8.5) for: (a–c) ECONUS, (d–f) Minneapolis, MN, (g–i) Amarillo, TX, and (j–l) Memphis, TN. Boxes represent the interquartile range, dots within the boxes are the means, lines within the boxes are medians, whiskers represent the 5th to 95th percentile range, and outliers denoted by unfilled circles. Significant differences—determined by a *p*-value less than 0.05 using the Mann-Whitney U test—between HIST and FUTR 4.5 (FUTR 8.5) are denoted by black diamonds (squares) above the maximum outliers.

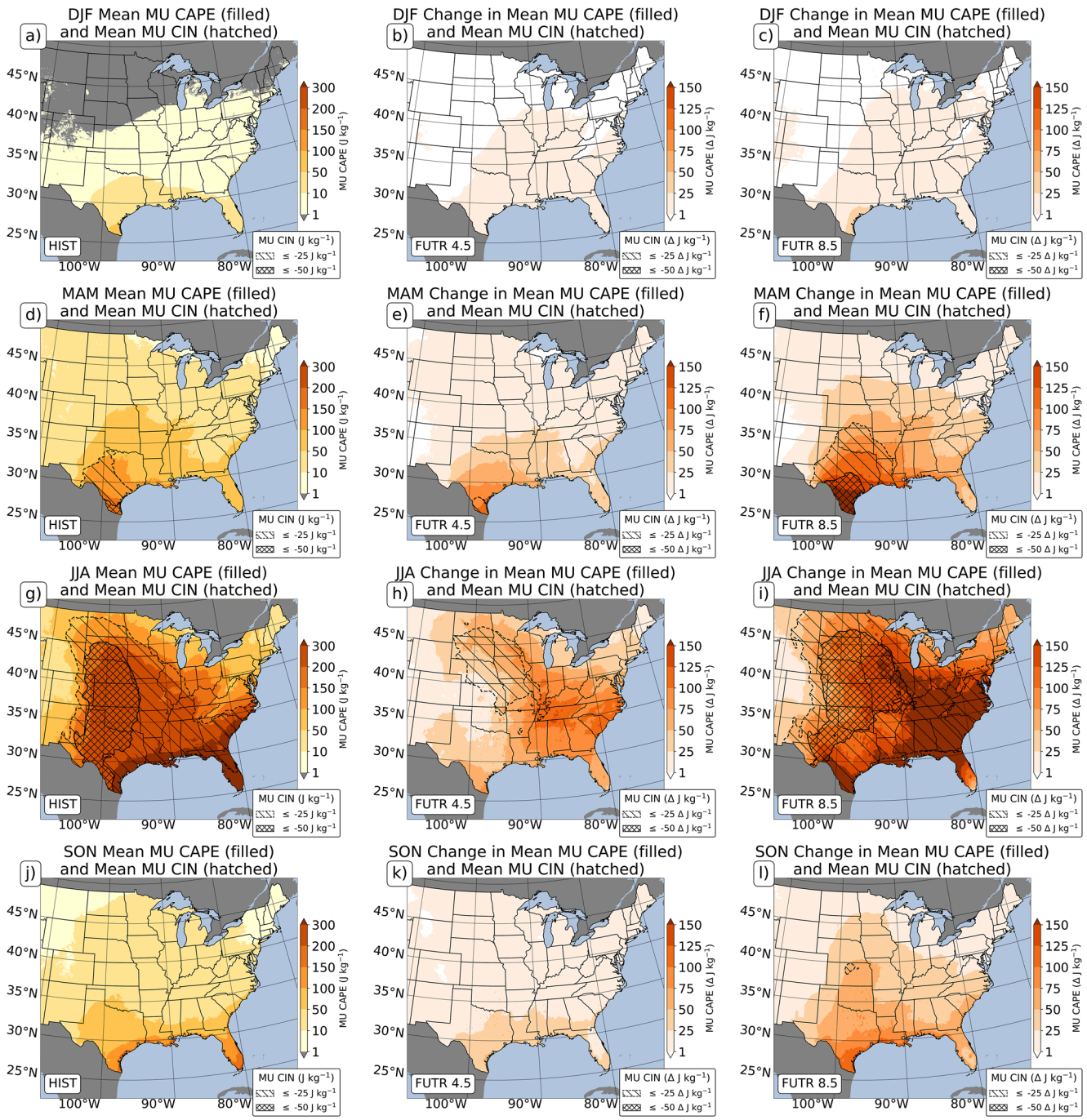

Figure 4. Mean seasonal MU CAPE (filled) and MU CIN (hatched) for HIST (first column), and mean seasonal changes in MU CAPE and MU CIN (relative to HIST) for FUTR 4.5 (second column) and FUTR 8.5 (third column). Hatches for mean seasonal MU CIN (left column) and changes (relative to HIST) in mean seasonal MU CIN (center and right columns) of <-25 J kg^{-1} and <-50 J kg^{-1} are denoted by lines and crosses, respectively. MU CIN is only considered if it is co-located with MU CAPE ≥ 100 J kg^{-1}.

6. Discussion and Conclusions

Although the response of thunderstorm activity to intermediate and extreme climate change scenarios was significant across the ECONUS for the vast majority of seasons and thresholds examined, regional changes varied. In general, most of the ECONUS saw significant decreases or no changes in annual 40 dBZ grid days. However, as the threshold was increased to 50 and 60 dBZ, most of the ECONUS saw either significant increases or no

changes in annual grid days. Notably, significant increases in annual thunderstorm activity were observed despite decreases (some significant) during the summer, which is the current peak of annual thunderstorm activity in the ECONUS (Changnon, 2001). Seasonal and regional analyses (Figure 3) revealed an overall increase in winter (Figure S1 in Supporting Information S1), fall (Figure S4 in Supporting Information S1) and spring (Figure S2 in Supporting Information S1) thunderstorm activity which appears to offset decreases during the summer (Figure S3 in Supporting Information S1) in FUTR 4.5 and 8.5. Potential seasonal shifts in the frequency of 40 dBZ grid days at the end of the century generally agree with those presented in existing literature (Rasmussen et al., 2020; Trapp et al., 2019). The results from higher thresholds (i.e., 50 and 60 dBZ) follow the hail-focused results in Trapp et al. (2019), and suggest that hail-specific variables from HIST, FUTR 4.5, and FUTR 8.5 should be examined in future work.

Cumulative mean thunderstorm days for the ECONUS were similar for 40 dBZ grid days in HIST, FUTR 4.5, and FUTR 8.5 (Figure 2a). However, at the higher thresholds of 50 and 60 dBZ (Figures 2b and 2c), both FUTR 4.5 and 8.5 produced more annual grid days. Further, there were more 50 and 60 dBZ grid days in FUTR 8.5 compared to FUTR 4.5. This pattern was not consistent within the examined sub regions. For example, Amarillo grids experienced fewer 40 and 50 dBZ grid days (Figures 2g and 2h) in FUTR 8.5 compared to both HIST and FUTR 4.5, which is the opposite of what occurred within the ECONUS as a whole. Minneapolis grids showed few differences between HIST and FUTR 4.5 for all thresholds, but experience more days in FUTR 8.5 (Figures 2d–2f), suggesting a step change in thunderstorm activity when the change in radiative forcing exceeds that produced by FUTR 4.5. Memphis grids largely mirrored the ECONUS results, except for larger relative differences in annual 50 and 60 dBZ grid days between HIST and the two climate change scenarios.

Seasonal comparisons between regions revealed varied responses to the two climate change scenarios. Overall, ECONUS grids experienced summertime decreases in 40 and 50 dBZ days, while seeing more 60 dBZ days (Figures 3a–3c). In contrast, fall, winter, and spring produced more 40, 50, and 60 dBZ grid days. As was the case with cumulative mean thunderstorm days, the examined regions did not always follow the same pattern. While Memphis (Figures 3k–3l) and Minneapolis (Figures 3d–3f) grids experienced increases in grid days during the spring, Amarillo (Figures 3g–3i) experienced decreases. Both Memphis and Minneapolis grid clusters had significant increases in 40, 50, and 60 dBZ grid days during the winter and fall. Interestingly, the smallest changes occurred during the summer for Amarillo, Memphis, and Minneapolis grids. This period also produced the most variability, as evidenced by the large interquartile ranges relative to other seasons. The results suggest the potential of a modified seasonal cycle of thunderstorm activity by the end of the 21st century. Memphis, for example, experiences a peak in 40, 50, and 60 dBZ grid day counts during the spring in future climate change scenarios, whereas HIST grid day counts peaked during the summer. On the other hand, Amarillo grids experienced a dampened seasonal cycle—namely, even though grid day counts peaked in the summer for HIST and the two climate change scenarios, the peak is lower than the one produced by HIST in both FUTR 4.5 and 8.5.

The varying responses of 40, 50, and 60 dBZ grid days to climate change scenarios are in line with results from works that have examined realized and possible changes in the character of rainfall (Brown et al., 2019; Prein et al., 2017; Trenberth et al., 2003) and hail (Trapp et al., 2019). Changes in MU CAPE and MU CIN (Figure 4) could be a driver of these changes—namely, the suppression of deep, moist convection becomes more likely as MU CIN increases, while larger MU CAPE results in more vigorous deep, moist convective updrafts when CIN is overcome (Trapp, 2013). Evidence supporting this hypothesis can be seen in the difference between late 21st century changes in 40 and 60 dBZ grid days. For all seasons and regions examined, 60 dBZ grid days are more common in the two end-of-century climate change scenarios, with many of these changes significant. And although 40 dBZ grid days generally increase or remain stationary for fall, winter, and spring, every region examined experienced decreases during the June - August period. The decreasing frequency of 40 dBZ grid days may be in response to a stronger capping during the summer, which may be the result of an increasingly arid western United States in FUTR 4.5 and 8.5 (Seager et al., 2018; Ting et al., 2018). Future work should explicitly examine the climatology of elevated mixed layers during the warm season to determine if these events are happening more often and are associated with stronger capping.

Data Availability Statement

The bias-corrected CESM data is archived at the following link: https://doi.org/10.5065/D6DJ5CN4. The code and data used for this work can be found at https://doi.org/10.5281/zenodo.6624592.

Acknowledgments
The authors would like to acknowledge high-performance computing support from Cheyenne (https://doi.org/10.5065/D6RX99HX) provided by NCAR's Computational and Information Systems Laboratory, sponsored by the National Science Foundation. This research was supported by the National Science Foundation award numbers 1637225 and 1800582. The authors also would like to acknowledge and thank Dr. Michael Papka (NIU/Argonne) and the Argonne Leadership Computing Facility at Argonne National Laboratory for data storage and post processing assistance. This research used resources of the Argonne Leadership Computing Facility, which is a DOE Office of Science User Facility supported under Contract DE-AC02-06CH11357.

References

Allen, J. T. (2018). Climate change and severe thunderstorms. In *Oxford research encyclopedia of climate science*.

Ashley, W. S., Bentley, M. L., & Stallins, J. A. (2012). Urban-induced thunderstorm modification in the Southeast United States. *Climatic Change*, *113*(2), 481–498. https://doi.org/10.1007/s10584-011-0324-1

Blair, S. F., Deroche, D. R., Boustead, J. M., Leighton, J. W., Barjenbruch, B. L., & Gargan, W. P. (2011). A radar-based assessment of the detectability of giant hail. *E-Journal of Severe Storms Meteorology*, *6*(7), 1–30.

Brooks, H. E. (2013). Severe thunderstorms and climate change. *Atmospheric Research*, *123*, 129–138. https://doi.org/10.1016/j.atmosres.2012.04.002

Brooks, H. E., Doswell, C. A., III, Zhang, X., Chernokulsky, A. A., Tochimoto, E., Hanstrum, B., et al. (2019). A century of progress in severe convective storm research and forecasting. *Meteorological Monographs*, *59*, 18–21. https://doi.org/10.1175/amsmonographs-d-18-0026.1

Brooks, H. E., Lee, J. W., & Craven, J. P. (2003). The spatial distribution of severe thunderstorm and tornado environments from global reanalysis data. *Atmospheric Research*, *67*, 73–94. https://doi.org/10.1016/s0169-8095(03)00045-0

Brown, V. M., Keim, B. D., & Black, A. W. (2019). Climatology and trends in hourly precipitation for the southeast United States. *Journal of Hydrometeorology*, *20*(8), 1737–1755. https://doi.org/10.1175/jhm-d-19-0004.1

Bruyère, C. L., Done, J. M., Holland, G. J., & Fredrick, S. (2014). Bias corrections of global models for regional climate simulations of high-impact weather. *Climate Dynamics*, *43*(7), 1847–1856. https://doi.org/10.1007/s00382-013-2011-6

Callendar, G. S. (1938). The artificial production of carbon dioxide and its influence on temperature. *Quarterly Journal of the Royal Meteorological Society*, *64*(275), 223–240. https://doi.org/10.1002/qj.49706427503

Changnon, S. A. (2001). Thunderstorm rainfall in the conterminous United States. *Bulletin of the American Meteorological Society*, *82*(9), 1925–1940. https://doi.org/10.1175/1520-0477(2001)082<1925:tritcu>2.3.co;2

Changnon, S. A., & Changnon, D. (2001). Long-term fluctuations in thunderstorm activity in the United States. *Climatic Change*, *50*(4), 489–503. https://doi.org/10.1023/a:1010651512934

Chen, J., Dai, A., Zhang, Y., & Rasmussen, K. L. (2020). Changes in convective available potential energy and convective inhibition under global warming. *Journal of Climate*, *33*(6), 2025–2050. https://doi.org/10.1175/jcli-d-19-0461.1

Creighton, G., Kuchera, E., Adams-Selin, R., McCormick, J., Rentschler, S., & Wickard, B. (2014). *AFWA diagnostics in WRF*. Citeseer.

Cummins, K. L., & Murphy, M. J. (2009). An overview of lightning locating systems: History, techniques, and data uses, with an in-depth look at the US NLDN. *IEEE Transactions on Electromagnetic Compatibility*, *51*(3), 499–518. https://doi.org/10.1109/temc.2009.2023450

Diffenbaugh, N. S., Scherer, M., & Trapp, R. J. (2013). Robust increases in severe thunderstorm environments in response to greenhouse forcing. *Proceedings of the National Academy of Sciences*, *110*(41), 16361–16366. https://doi.org/10.1073/pnas.1307758110

Doswell, C. A., III., & Schultz, D. M. (2006). On the use of indices and parameters in forecasting severe storms. *E-Journal of Severe Storms Meteorology*, *1*(3), 1–22.

Fabry, F., Meunier, V., Treserras, B. P., Cournoyer, A., & Nelson, B. (2017). On the climatological use of radar data mosaics: Possibilities and challenges. *Bulletin of the American Meteorological Society*, *98*(10), 2135–2148. https://doi.org/10.1175/bams-d-15-00256.1

Geerts, B., Parsons, D., Ziegler, C. L., Weckwerth, T. M., Biggerstaff, M. I., Clark, R. D., et al. (2017). The 2015 plains elevated convection at night field project. *Bulletin of the American Meteorological Society*, *98*(4), 767–786. https://doi.org/10.1175/bams-d-15-00257.1

Gensini, V. A. (2021). Severe convective storms in a changing climate. In *Climate change and extreme events* (pp. 39–56). Elsevier.

Gensini, V. A., & Ashley, W. S. (2011). Climatology of potentially severe convective environments from the North American Regional Reanalysis. *E-Journal of Severe Storms Meteorology*, *6*(8), 1–40.

Gensini, V. A., & Brooks, H. E. (2018). Spatial trends in United States tornado frequency. *NPJ climate and atmospheric science*, *1*(1), 1–5. https://doi.org/10.1038/s41612-018-0048-2

Gensini, V. A., Haberlie, A. M., & Ashley, W. S. (2022). Convection-permitting simulations of historical and possible future climate over the contiguous United States. *Climate Dynamics*, 1–18. https://doi.org/10.1007/s00382-022-06306-0

Gensini, V. A., & Mote, T. L. (2014). Estimations of hazardous convective weather in the United States using dynamical downscaling. *Journal of Climate*, *27*(17), 6581–6589. https://doi.org/10.1175/jcli-d-13-00777.1

Gensini, V. A., & Mote, T. L. (2015). Downscaled estimates of late 21st century severe weather from CCSM3. *Climatic Change*, *129*(1), 307–321. https://doi.org/10.1007/s10584-014-1320-z

Gensini, V. A., Ramseyer, C., & Mote, T. L. (2014). Future convective environments using NARCCAP. *International Journal of Climatology*, *34*(5), 1699–1705. https://doi.org/10.1002/joc.3769

Hartmann, D. L. (2015). *Global physical climatology* (Vol. 103). Elsevier.

Hoogewind, K. A., Baldwin, M. E., & Trapp, R. J. (2017). The impact of climate change on hazardous convective weather in the United States: Insight from high-resolution dynamical downscaling. *Journal of Climate*, *30*(24), 10081–10100. https://doi.org/10.1175/jcli-d-16-0885.1

Hurrell, J. W., Holland, M. M., Gent, P. R., Ghan, S., Kay, J. E., Kushner, P. J., et al. (2013). The community Earth system model: A framework for collaborative research. *Bulletin of the American Meteorological Society*, *94*(9), 1339–1360. https://doi.org/10.1175/bams-d-12-00121.1

Kendon, E., Prein, A., Senior, C., & Stirling, A. (2021). Challenges and outlook for convection-permitting climate modelling. *Philosophical Transactions of the Royal Society A*, *379*, 20190547. https://doi.org/10.1098/rsta.2019.0547

Klazura, G. E., & Imy, D. A. (1993). A description of the initial set of analysis products available from the NEXRAD WSR-88D system. *Bulletin of the American Meteorological Society*, *74*(7), 1293–1312. https://doi.org/10.1175/1520-0477(1993)074<1293:adotis>2.0.co;2

Koehler, T. L. (2020). Cloud-to-ground lightning flash density and thunderstorm day distributions over the contiguous United States derived from NLDN measurements: 1993–2018. *Monthly Weather Review*, *148*(1), 313–332. https://doi.org/10.1175/mwr-d-19-0211.1

Lepore, C., Abernathey, R., Henderson, N., Allen, J. T., & Tippett, M. K. (2021). *Future global convective environments in CMIP6 models*. Earth's Future, 9(12), e2021EF002277.

Liu, C., Ikeda, K., Rasmussen, R., Barlage, M., Newman, A. J., Prein, A. F., et al. (2017). Continental-scale convection-permitting modeling of the current and future climate of North America. *Climate Dynamics*, *49*(1), 71–95. https://doi.org/10.1007/s00382-016-3327-9

McNulty, R. P. (1995). Severe and convective weather: A central region forecasting challenge. *Weather and Forecasting*, *10*(2), 187–202. https://doi.org/10.1175/1520-0434(1995)010<0187:sacwac>2.0.co;2

Menzel, W. P., & Purdom, J. F. (1994). Introducing GOES-I: The first of a new generation of geostationary operational environmental satellites. *Bulletin of the American Meteorological Society*, *75*(5), 757–782. https://doi.org/10.1175/1520-0477(1994)075<0757:igitfo>2.0.co;2

Miguez-Macho, G., Stenchikov, G. L., & Robock, A. (2004). Spectral nudging to eliminate the effects of domain position and geometry in regional climate model simulations. *Journal of Geophysical Research*, *109*(D13), D13104. https://doi.org/10.1029/2003jd004495

Monaghan, A., Steinhoff, D., Bruyere, C., & Yates, D. (2014). *NCAR CESM global bias-corrected CMIP5 output to support WRF/MPAS research*. Research Data Archive National Center Atmospheric Research Computational Information Systems Laboratory.

Moss, R. H., Edmonds, J. A., Hibbard, K. A., Manning, M. R., Rose, S. K., Van Vuuren, D. P., et al. (2010). The next generation of scenarios for climate change research and assessment. *Nature*, *463*(7282), 747–756. https://doi.org/10.1038/nature08823

Ortega, K. L. (2018). Evaluating multi-radar, multi-sensor products for surface hailfall diagnosis. *E-Journal of Severe Storms Meteorology*, *13*(1), 1–36.

Pachauri, R. K., Allen, M. R., Barros, V. R., Broome, J., Cramer, W., Christ, R., et al. (2014). *Climate change 2014: Synthesis report. Contribution of Working Groups I, II and III to the fifth assessment report of the Intergovernmental Panel on Climate Change*. IPCC.

Parker, M. D., & Knievel, J. C. (2005). Do meteorologists suppress thunderstorms?: Radar-derived statistics and the behavior of moist convection. *Bulletin of the American Meteorological Society*, *86*(3), 341–358. https://doi.org/10.1175/bams-86-3-341

Prein, A. F., Langhans, W., Fosser, G., Ferrone, A., Ban, N., Goergen, K., et al. (2015). A review on regional convection-permitting climate modeling: Demonstrations, prospects, and challenges. *Reviews of Geophysics*, *53*(2), 323–361. https://doi.org/10.1002/2014rg000475

Prein, A. F., Rasmussen, R. M., Ikeda, K., Liu, C., Clark, M. P., & Holland, G. J. (2017). The future intensification of hourly precipitation extremes. *Nature Climate Change*, *7*(1), 48–52. https://doi.org/10.1038/nclimate3168

Rasmussen, K. L., Prein, A. F., Rasmussen, R. M., Ikeda, K., & Liu, C. (2020). Changes in the convective population and thermodynamic environments in convection-permitting regional climate simulations over the United States. *Climate Dynamics*, *55*(1), 383–408. https://doi.org/10.1007/s00382-017-4000-7

Riemann-Campe, K., Fraedrich, K., & Lunkeit, F. (2009). Global climatology of convective available potential energy (CAPE) and convective inhibition (CIN) in ERA-40 reanalysis. *Atmospheric Research*, *93*(1–3), 534–545. https://doi.org/10.1016/j.atmosres.2008.09.037

Seager, R., Lis, N., Feldman, J., Ting, M., Williams, A. P., Nakamura, J., et al. (2018). Whither the 100th meridian? The once and future physical and human geography of America's arid–humid divide. Part I: The story so far. *Earth Interactions*, *22*(5), 1–22. https://doi.org/10.1175/ei-d-17-0011.1

Serafin, R. J., & Wilson, J. W. (2000). Operational weather radar in the United States: Progress and opportunity. *Bulletin of the American Meteorological Society*, *81*(3), 501–518. https://doi.org/10.1175/1520-0477(2000)081<0501:owritu>2.3.co;2

Skamarock, W. C., Klemp, J. B., Dudhia, J., Gill, D. O., Liu, Z., Berner, J., et al. (2019). *A description of the advanced research WRF model version 4* (Vol. 145). National Center for Atmospheric Research.

Smith, J. A., Seo, D. J., Baeck, M. L., & Hudlow, M. D. (1996). An intercomparison study of NEXRAD precipitation estimates. *Water Resources Research*, *32*(7), 2035–2045. https://doi.org/10.1029/96wr00270

Stevenson, S. N., & Schumacher, R. S. (2014). A 10-year survey of extreme rainfall events in the central and eastern United States using gridded multisensor precipitation analyses. *Monthly Weather Review*, *142*(9), 3147–3162. https://doi.org/10.1175/mwr-d-13-00345.1

Stoelinga, M. T. (2005). Simulated equivalent reflectivity factor as currently formulated in RIP: Description and possible improvements. *White paper* (p. 5).

Takayabu, I., Rasmussen, R., Nakakita, E., Prein, A., Kawase, H., Watanabe, S., et al. (2021). Convection-permitting models for climate research. *Bulletin of the American Meteorological Society*, *1*, E77–E12. https://doi.org/10.1175/bams-d-21-0043.1

Tang, B. H., Gensini, V. A., & Homeyer, C. R. (2019). Trends in United States large hail environments and observations. *NPJ Climate and Atmospheric Science*, *2*(1), 1–7. https://doi.org/10.1038/s41612-019-0103-7

Taszarek, M., Allen, J., Brooks, H., Pilguj, N., & Czernecki, B. (2021). Differing trends in United States and European severe thunderstorm environments in a warming climate. *Bulletin of the American Meteorological Society*, *102*(2), E296–E322. https://doi.org/10.1175/bams-d-20-0004.1

Taszarek, M., Allen, J., Marchio, M., & Brooks, H. (2021). Global climatology and trends in convective environments from ERA5 and rawinsonde data. *npj Climate and Atmospheric Science*, *4*(1), 1–11. https://doi.org/10.1038/s41612-021-00190-x

Taszarek, M., Allen, J. T., Púčik, T., Hoogewind, K. A., & Brooks, H. E. (2020). Severe convective storms across Europe and the United States. Part II: ERA5 environments associated with lightning, large hail, severe wind, and tornadoes. *Journal of Climate*, *33*(23), 10263–10286. https://doi.org/10.1175/jcli-d-20-0346.1

Ting, M., Seager, R., Li, C., Liu, H., & Henderson, N. (2018). Mechanism of future spring drying in the southwestern United States in CMIP5 models. *Journal of Climate*, *31*(11), 4265–4279. https://doi.org/10.1175/jcli-d-17-0574.1

Trapp, R. J. (2013). *Mesoscale-convective processes in the atmosphere*. Cambridge University Press.

Trapp, R. J., Diffenbaugh, N. S., Brooks, H. E., Baldwin, M. E., Robinson, E. D., & Pal, J. S. (2007). Changes in severe thunderstorm environment frequency during the 21st century caused by anthropogenically enhanced global radiative forcing. *Proceedings of the National Academy of Sciences*, *104*(50), 19719–19723. https://doi.org/10.1073/pnas.0705494104

Trapp, R. J., Diffenbaugh, N. S., & Gluhovsky, A. (2009). Transient response of severe thunderstorm forcing to elevated greenhouse gas concentrations. *Geophysical Research Letters*, *36*(1), L01703. https://doi.org/10.1029/2008gl036203

Trapp, R. J., Halvorson, B. A., & Diffenbaugh, N. S. (2007). Telescoping, multimodel approaches to evaluate extreme convective weather under future climates. *Journal of Geophysical Research*, *112*(D20), D20109. https://doi.org/10.1029/2006jd008345

Trapp, R. J., Hoogewind, K. A., & Lasher-Trapp, S. (2019). Future changes in hail occurrence in the United States determined through convection-permitting dynamical downscaling. *Journal of Climate*, *32*(17), 5493–5509. https://doi.org/10.1175/jcli-d-18-0740.1

Trapp, R. J., Robinson, E. D., Baldwin, M. E., Diffenbaugh, N. S., & Schwedler, B. R. (2011). Regional climate of hazardous convective weather through high-resolution dynamical downscaling. *Climate Dynamics*, *37*(3), 677–688. https://doi.org/10.1007/s00382-010-0826-y

Trenberth, K. E., Dai, A., Rasmussen, R. M., & Parsons, D. B. (2003). The changing character of precipitation. *Bulletin of the American Meteorological Society*, *84*(9), 1205–1218. https://doi.org/10.1175/bams-84-9-1205

Weisman, M. L., Skamarock, W. C., & Klemp, J. B. (1997). The resolution dependence of explicitly modeled convective systems. *Monthly Weather Review*, *125*(4), 527–548. https://doi.org/10.1175/1520-0493(1997)125<0527:trdoem>2.0.co;2